Sensorless Planning for Medical Needle Insertion Procedures*

Ron Alterovitz and Ken Goldberg
IEOR & EECS Departments
University of California, Berkeley

Jean Pouliot, Richard Taschereau, and I-Chow Hsu
Department of Radiation Oncology
University of California, San Francisco

Abstract **– Medical procedures such as seed implants, biopsies, and treatment injections require inserting a needle tip to a specific target location inside the human body. This is difficult because (1) insertion causes soft tissues to displace and deform, and (2) it is often difficult or impossible to obtain imaging data during insertion. We are developing a sensorless planning system for needle insertion that incorporates numerical optimization and a soft tissue simulation based on finite element methods. The simulation, based on a dynamic FEM formulation, models the effects of needle tip and frictional forces on soft tissues defined by a 2D mesh. In this paper we describe a sensorless planning algorithm for radioactive seed implantation that computes needle offsets to minimize seed placement error. The resulting needle offsets compensate for predicted tissue deformations without real-time imaging.**

I. INTRODUCTION

Medical procedures such as brachytherapy, biopsy, and treatment injections require inserting a needle to a specific target location inside the body to implant a radioactive seed, extract a tissue sample, or inject a drug. In all cases, the needle tip should be as close as possible to an internal target when the procedure is performed. Unfortunately, inserting the needle causes the surrounding soft tissues to displace and deform. Real-time imaging is often not available during insertion or is of very poor quality. As illustrated in Fig. 1 left column, lack of planning can result in substantial *placement error*.

We are developing a sensorless planning system for needle insertion to reduce placement error. We use a 2D FEM model of the soft tissues surrounding the target implant location and then use dynamic simulation of needle insertion to compute tissue deformations. The simulation is repeated for different insertion locations and depths to compute an optimal set of needle offsets: a sensorless motion plan as illustrated in Fig. 1 right column greatly reduced placement error.

In this paper we demonstrate the system in the context of permanent seed prostate brachytherapy, a minimally invasive medical procedure that is widely used for treating prostate cancer. During the procedure, physicians use needles to permanently implant radioactive seeds inside the prostate that irradiate the surrounding tissue over several months. The radioactive dose delivered should minimize healthy tissue damage while maximizing the destruction of cancerous cells. The success of this procedure depends on the accurate placement of radioactive seeds within the prostate gland [11, 22].

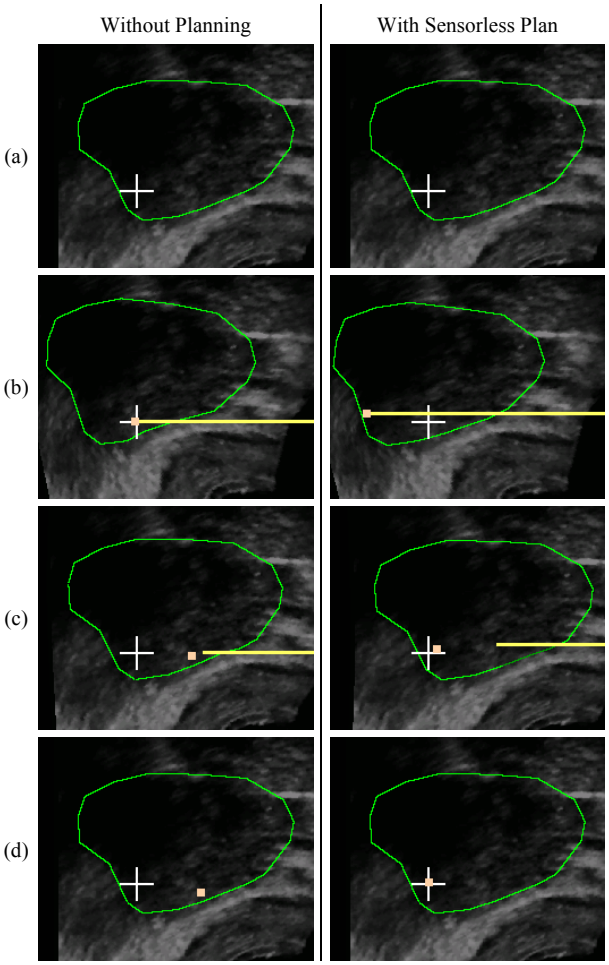

Fig. 1: Four vertical frames illustrating needle insertion based on deforming ultrasound images of the human prostate using simulation. The left column shows results without planning, producing substantial placement error. The right column shows results with the sensorless plan, with minimal placement error. The target implant location is indicated in all frames with a white cross fixed in the external body frame. Frame (a) outlines the prostate. In Frame (b), the needle is inserted to the target without planning and past the target by a computed offset with the sensorless plan; in both cases the radioactive seed (small square) is released at the needle tip. In Frame (c), the needle is retracted. Frame (d) indicates the resulting *placement error*, the distance between the target and resulting seed location. Without planning, placement error is substantial: 26% of the width of the prostate resulting in damage to healthy tissue and failure to kill cancerous cells. With sensorless planning, shown in the right image of Frame (d), placement error is negligible.

* Submitted to IEEE/RSJ International Conference on Intelligent Robots and Systems, Las Vegas, NV, October 2003. For more information, please contact *ron@ieor.berkeley.edu* or *goldberg@ieor.berkeley.edu* or visit *http://alpha.ieor.berkeley.edu/ron/research*.

Before the implant procedure, a dosimetric plan is prepared based on static imaging of the prostate and medical considerations. Methods for calculating optimal seed locations are available [23, 19, 30]. Achieving the desired seed placement in the patient is left to the physician. Multiple seeds and biodegradable spacers are loaded into needles that the physician inserts transperineally into the patient who is lying on his back. Seeds and spacers are ejected from the needle when the depth specified by the dosimetric plan is reached.

Tissue deformations during the implantation contribute to seed misplacement [22, 26], as simulated in Fig. 1. In prior work, an experienced physician implanting 1195 seeds in 30 patients achieved average displacement errors of 0.47cm in depth and 0.22cm in height for an average placement error of 0.63cm [26], which is a substantial error of 21% for prostates that average 3cm in width. Although real-time ultrasound imaging is available during the procedure, it does not produce crisp tissue boundaries and cannot be used to precisely track the penetration of the needle into the deformed prostate. Below we describe a sensorless planning approach that can greatly reduce seed placement error without real-time imaging.

II. Related Work

In robotics, sensorless planning algorithms, pioneered by Mason and Erdmann in the 1980s [13], have been developed to position and orient mechanical parts using parallel jaws [15], vibrating surfaces [7], and squeeze and roll primitives for micro-scale parts [20]. Sensorless planning has also been applied to insertion of parts inside fixtures [5] and moving parts across surfaces [10].

To apply sensorless planning to needle insertion, we require a fast and accurate simulation. DiMaio and Salcudean performed pioneering work in simulating the deformations that occur during needle insertion [12]. Their simulation, based on a quasi-static finite element method, achieves extremely fast update rates (500Hz) and high accuracy (node displacement error of 1.4mm for needle penetration of 70mm). High accuracy requires a calibration phase where the force distribution along the needle shaft is estimated based on observed tissue deformations. This force distribution, which is modeled with a parameterized surface in Figure 11 of [12], may be difficult to measure in vivo. Our simulation uses an alternative model based on a reduced set of scalar parameters such as needle friction, sharpness, and velocity [2]. The sensitivity of current medical methods to these simulation parameters was analyzed in [2]. In this paper, we focus on sensorless planning: computing offsets for insertion height and depth to minimize placement error.

Needle insertion simulation requires computing deformations of soft tissue when forces are applied. The history of offline animation and real-time simulation of deformable objects is summarized in [14]. Unlike heuristic methods like the mass-spring model, the finite element method (FEM) is based on the equations of continuum mechanics. The feasibility and potential of this approach for animation was demonstrated by Terzopolous et al. [28]. Real-time visual performance for surgery simulation of the human liver using FEM was achieved by Stéphane Cotin et al. using a large preprocessing step [9]. They modeled tissue as a linearly elastic material and allowed only small quasi-static deformations.

Our simulator relaxes the quasi-static assumption and simulates dynamic deformations, as formulated by Zhuang [31] and Picinbono et al. [20]. These dynamic simulations rely on mass lumping to achieve interactive performance, but the loss of realism for soft tissues resulting from this approximation is relatively low as shown experimentally in [3]. Both Zhuang and Picinbono et al. use quadratic strain to accurately model large deformations, and Wu et al. extended this work to include nonlinear material elasticity [29].

Setting accurate parameters for tissue properties is important for realistic simulation. We use results from Krouskop et al., who estimated the elastic modulus for prostate and breast tissue using ultrasonic imaging [18]. Recent work in nonlinear parameter estimation includes [8] and [16]. Kataoka et al. separately measured tip and frictional forces during needle insertion into a canine prostate, which is useful for simulation validation [25].

When real-time sensor data such as imaging is available during needle insertion procedures, robotic control algorithms can be used to steer the needle to the desired target [24]. However, sensorless planning must be used when real-time sensor data is not available or unreliable.

Sensorless planning based on pre-operatively predicting the effects of tissue deformations has been used for some medical procedures. In [4], a piece-wise nonlinear FEM model was used to track the position of a tumor during breast compression before a breast cancer biopsy. Statistical and FEM methods that approximated tissue deformations caused by uniform force loading are compared in [17] for biopsy applications. However, we are not aware of past work explicitly simulating needle insertion and the resulting tissue deformations to plan needle procedures without real-time sensor input.

III. Problem Definition

Given a target point for the seed, we compute a needle insertion plan that will minimize *placement error*, the distance between the needle tip and a target location within the tissue. In 2D, we must compute a needle insertion height $\bar{y}$ and a depth $\bar{z}$ so that the needle tip reaches a point (y, z) as close as possible to the target location (y_t, z_t) inside the tissue. Based on brachytherapy,

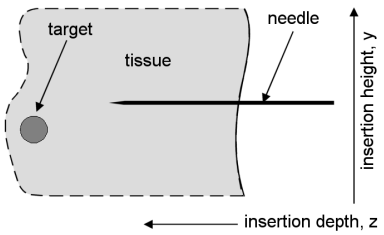

Fig. 2: In 2D, insertion height and depth should be set so that the needle tip reaches the target with minimum placement error. The target's location in the world frame moves as the needle is inserted because the tissue is deformed.

we refer to the actual location in the tissue (y, z) reached by the needle tip as the seed placement, although this could refer to a biopsy or injection location.

Input:

G: Tissue reference mesh with material properties

(y_t, z_t): Target coordinate in the tissue

$(\bar{y}_{min}, \bar{y}_{max})$: Range of feasible insertion heights

$\bar{z}_{max}$: Maximum feasible insertion depth

v: Needle velocity during insertion and retraction

h: FEM simulation time step

Output:

E^*: Minimum feasible placement error

$(\bar{y}^*, \bar{z}^*)$: Insertion height and depth to obtain error E^*

Our planning algorithm for needle procedures is composed of the following stages:

1. *Tissue Model*: Create a model of the deformable tissues surrounding the target implant location.
2. *Simulating Needle Insertion*: Given a needle insertion height and depth, simulate needle insertion to compute seed placement and error.
3. *Needle Insertion Planning*: Optimize the insertion height and depth to minimize placement error.

These steps are explained in sections IV, V, and VI below. We then apply our system to prostate brachytherapy in section VII.

IV. Soft Tissue Model

A. Tissue Geometry

The soft tissues surrounding the target are defined using a mesh composed of m discrete 3-node triangular elements created using n total nodes, each with 2 degrees of freedom. This *reference mesh* G defines the geometry of the tissues, with each node's coordinate stored in the position vector $\mathbf{x}$. The simulation computes mesh deformations that simulate the tissue's response to the needle. The *deformed mesh* $\bar{G}$ *is* constructed using the node coordinates $\mathbf{x}+\mathbf{u}$ in the world frame, where $\mathbf{u}$ is the nodal displacement vector, as shown in Fig. 3.

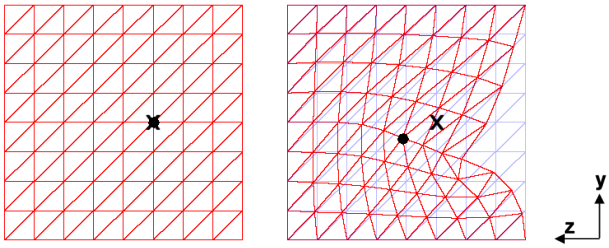

(a) (b)

Fig. 3: The coordinate of the target in the reference mesh (y_t, z_t), denoted by ×, coincides with the target in the world frame $(\bar{y}_t, \bar{z}_t)$, denoted by • (a). Both the × and • represent the same location within the tissue, but their world frame coordinates differ when the tissue is deformed (b).

B. Computing Soft Tissue Deformations

We use the finite element method (FEM) to compute the deformations of soft tissues when forces are applied by the needle. Rather than calculating only static deformations, we simulate the dynamic behavior of soft tissues by solving for the acceleration, velocity, and displacement of each node for every time step to produce a history-dependant simulation.

We approximate soft tissues as linearly elastic materials. The FEM problem for mesh G is defined by a system of up to $d=2n$ linear differential equations:

$$\mathbf{M}\,\mathbf{a}_i + \mathbf{C}\,\mathbf{v}_i + \mathbf{K}\,\mathbf{u}_i = \mathbf{f}_i \qquad (1)$$

where $\mathbf{M}$ is the mass matrix, $\mathbf{C}$ is the damping matrix, $\mathbf{K}$ is the stiffness matrix, $\mathbf{f}_i$ is the external force vector, $\mathbf{a}_i$ is the nodal acceleration vector, $\mathbf{v}_i$ is the nodal velocity vector, and $\mathbf{u}_i$ is the nodal displacement vector at time step i [32].

To integrate the differential system (1) over time, we use the Newmark method, which translates the differential system into a linear system of equations. We solve this system using the methods shown in [2] for interactive performance.

V. Simulating Needle Insertion

We assume that the needle is thin and rigid. The world frame is rotated so that the needle is being inserted along the z-axis and the insertion height is determined by the y-axis. Once the needle is in contact with tissue, we assume the needle's y-coordinate is fixed and it only moves parallel to the horizontal z-axis.

Our simulation extends the model and algorithm in [2] to support meshes with nonhomogeneous material properties. The algorithm simulates the force the needle exerts on the tissue at its tip and frictional forces along the needle shaft. Puncturing tissue membranes requires additional force at the needle tip. These forces applied by the needle are computed and the FEM force vector $\mathbf{f}_i$ is updated at every time step.

Using FEM, forces are applied as boundary conditions on elements in the reference mesh. Since the physician may insert the needle at any location, it is usually necessary to modify the reference mesh in real-time to ensure that element boundaries are present where the tip and friction forces must be applied. To apply the tip force, a node is maintained at the needle tip location during insertion. To apply the friction forces, a list of nodes along the needle shaft is maintained and these nodes are constrained to only move horizontally along the needle shaft. These mesh modifications are fully described in [2].

A seed can be implanted at the location of the needle tip in the reference mesh at any time. We assume that the seed does not move in the reference mesh after it is implanted. The location of the seed is tracked efficiently by storing in memory the containing element of the seed in the reference mesh and updating it if any nodes of the containing element are moved. The seed's world frame coordinates are computed by interpolating between the enclosing element's deformed node coordinates.

VI. NEEDLE INSERTION PLANNING

A needle insertion plan is defined by $(\bar{y}, \bar{z})$, where the needle is inserted at some height $\bar{y}$ to a depth $\bar{z}$ in the world frame. Since needles can only be inserted in certain locations on the skin surface, we define the feasible insertion height domain by $\bar{y} \in (\bar{y}_{min}, \bar{y}_{max})$. The maximum medically feasible insertion depth is given by $\bar{z}_{max}$.

The target location is (y_t, z_t) in the reference mesh. Given a plan $(\bar{y}, \bar{z})$, we can simulate needle insertion to compute the reference mesh coordinate (y, z) of the implanted seed. The goal is to find $(\bar{y}^*, \bar{z}^*)$ such that the corresponding reference mesh coordinate (y^*, z^*) equals (y_t, z_t); the seed should be implanted at the target in the reference mesh. The placement error E is defined by the Euclidean distance from (y^*, z^*) to (y_t, z_t).

Minimizing E can be broken down into two optimization problems, finding the optimal $\bar{z}^*$ given $\bar{y}^*$, and then finding the globally optimal $\bar{y}^*$.

A. Optimizing Needle Insertion Depth

When any $\bar{y}$ is given, we simulate needle insertion at height $\bar{y}$ to find $\bar{z}^*$ that minimizes E. The needle insertion simulation algorithm described in section V always maintains a node at the location the needle tip. If a seed is implanted at time step i, then the seed would be located at the coordinate of the tip node, which is $\mathbf{p}=(y_p, z_p)$ in the reference mesh. Hence, E is quickly computed as:

$$E = \sqrt{(y_p - y_t)^2 + (z_p - z_t)^2} .$$

We simulate needle insertion until the needle tip reaches $\bar{z}_{max}$ computing E for every time step and saving the $\bar{z}^*$ for which E is smallest.

This optimization takes $O(F\,\bar{z}_{max}/(v\,h))$ time in the worst case, where h is the time step duration, v is the needle velocity, and F is the complexity of the simulation solving algorithm described in section IV.B, which is $O(n)$ for interactive simulation. Since the needle tip will move a distance $v\,h$ each time step, the resolution of $\bar{z}^*$ is $v\,h$. A small h is desirable to improve the resolution of $\bar{z}^*$, but the number of time steps required to compute the optimal insertion depth $\bar{z}^*$ grows linearly as h decreases.

B. Improving Performance Using Adaptive Time Steps

Both the speed and precision of the planner can be improved using adaptive time steps. When the needle tip is far from the target, a large time step h_L should be used since the value of $\bar{z}^*$ will not affected. When the needle tip is close to the target, a small time step duration $h_S < h_L$ is desirable since $\bar{z}^*$ might be modified.

Although the needle tip moves exactly a distance $h\,v$ along the z-axis in the world frame, its movement in the reference mesh may be erratic as the needle cuts through tissue. To determine the optimal time to transition from h_L to h_S, we use parameters from the needle insertion algorithm defined in section V. The needle tip, located at point $\mathbf{p}_i$ in the reference mesh at time step i, moves in direction $\mathbf{r}_i$. If the needle tip force exceeds f_b, the tip will cut a length b of tissue and move to point $\mathbf{p}_{i+1}=\mathbf{p}_i+b\mathbf{r}_i$. The magnitude of parameter b is scaled by the factor $h\,v$. We use this to determine the time step duration. In Fig. 4, line l_1 connects points $\mathbf{p}_i$ and $\mathbf{p}_{i+1}$, and line l_2 is perpendicular to l_1 and passes through the target point $\mathbf{t}$. When l_1 intersects l_2 along the segment $(\mathbf{p}_i, \mathbf{p}_{i+1})$, a smaller time step is used in order to reduce the granularity $h\,v$ of $\bar{z}^*$ and decrease the distance between $\mathbf{p}_i$ and $\mathbf{p}_{i+1}$ so that a more precise optimal point can be found.

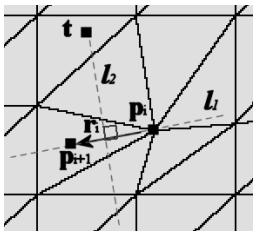

Fig. 4: When using adaptive time steps, a small time step will be used when the needle tip $\mathbf{p}_i$ is close to the target $\mathbf{t}$. The needle is heading in direction $\mathbf{r}_i$ to point $\mathbf{p}_{i+1}$ in the reference mesh. When l_1 intersects l_2 along the segment $(\mathbf{p}_i, \mathbf{p}_{i+1})$, a smaller time step is used in order to reduce the distance between $\mathbf{p}_i$ and $\mathbf{p}_{i+1}$ so that a more precise optimal point can be found.

C. Optimizing Needle Insertion Height

Due to tissue deformations during insertion, the needle tip position y in the reference mesh may not be the same as the needle insertion height $\bar{y}$. For a given $\bar{y}$, we can compute the minimum E and corresponding $\bar{z}^*$ using the approach in section VI.A. To find the optimal $\bar{y}^*$, we need to minimize the value of E as a function of $\bar{y}$.

Minimizing E as a function of $\bar{y}$ is difficult because derivative values are not available and E is not guaranteed to be unimodal (strictly quasiconvex) because of tissue

nonhomogeneity, tissue-bone connections, and other anatomical constraints. Hence, global optimality cannot be verified without analyzing the entire feasible space. In general, an approximate minimum of E can be found using a grid search over $\bar{y} \in (\bar{y}_{min}, \bar{y}_{max})$. For some simulations, it is not possible to insert the needle at different heights and still reach the same point inside the tissue (as in a square box of homogeneous tissue, for example). In such cases, E will be unimodal and a line search method such as the golden section method [6] can be used over the range $\bar{y} \in (\bar{y}_{min}, \bar{y}_{max})$ to find the optimal $\bar{y}^*$. Even when E is not unimodal, a line search method can still be used to find a locally optimal $\bar{y}^*$ that is better than the standard procedure $(\bar{y}_t, \bar{z}_t)$ that ignores deformations.

D. The Planning Algorithm

Algorithm input and output are defined in section III.

Helper functions:

GetOptimalDepth($\bar{y}$, G): Use model G and insertion height $\bar{y}$ to compute the optimal insertion depth and resulting seed placement as described in section VI.A.

NewLineSearchPoint($\bar{y}$): Returns a new $\bar{y}$ using a line search method as described in section VI.C.

Distance($\mathbf{p}_1$, $\mathbf{p}_2$): Euclidean distance between 2 points.

Pseudocode:

1. Initialize: $E = \infty$, $\bar{y} = y_t$, $\bar{z} = x_t$.
2. Repeat
3. $(\bar{z}, y, z)$ = GetOptimalDepth($\bar{y}$, G)
4. if(Distance((y, z), (y_t, z_t)) < E)
5. E = Distance((y, z), (y_t, z_t))
6. $\bar{z}^* = \bar{z}$, $\bar{y}^* = \bar{y}$
7. $\bar{y}$ = NewLineSearchPoint($\bar{y}$)
8. While(E > error_tolerance)
9. Return $(E, \bar{y}, \bar{z})$

VII. Planning for Prostate Brachytherapy

Fig. 1 provides a simulated case study showing that deformations can produce significant errors in final seed placements during prostate brachytherapy. Seed placement error should be minimized to achieve the optimal radioactive dose distribution. Since we assume the tissue is elastic and that the seed does not move in the reference frame once it is implanted, the placement error in the reference mesh at the time of implantation is the same as the distance between the target and seed in the prostate after needle retraction and tissue settling. Hence, the planning algorithm defined in section VI is sufficient to achieve the desired seed placement and we do not need to simulate needle retraction to compute the error.

A. Simulation Implementation

Our needle insertion simulator was implemented using C++ and OpenGL and tested on a 750MHz Pentium III PC with 256MB RAM. When executed in interactive simulation mode, a physician can guide the needle and implant seeds using a mouse. For a model with 1250 triangular elements the simulator responds at the rate of 24 frames per second, sufficient for visual feedback (but not fast enough for haptic control).

B. Prostate Model

Our prostate model is based on a patient who underwent brachytherapy treatment for prostate cancer at the UCSF Medical Center in June 2002. A static pre-procedure ultrasound image of the prostate was superimposed as a texture map on a mesh composed of 1250 triangular elements. A polygon outlining the prostate membrane was manually drawn on the texture map; underlying mesh elements within this polygon were assigned prostate tissue properties and the remaining elements were assigned fatty tissue properties. The Young's modulus and Poisson ratio were set using the results of [15]. During simulation, the static pre-procedure ultrasound image is deformed based on the underlying mesh and is displayed to the user.

To set the remaining simulation parameters and validate our model, we compared the output of the simulation with an ultrasound video recorded during a real medical procedure on the same patient in June 2002. The procedure was recorded using an ultrasound probe in the sagittal plane. Unknown model parameters were set so that the simulation output closely matched the ultrasound video. Snapshots from the simulation output were compared with frames from the ultrasound video [1]. Although it is difficult for non-specialists to identify gland boundaries in ultrasound, UCSF medical experts comparing the two image sequences judged them as remarkably similar. We plan to perform controlled experiments to further evaluate simulation accuracy across multiple patients.

C. Target Test Case

We test our planning algorithm using the target (y_t, z_t) = (1.50cm, 3.00cm) shown in Fig. 1 for a 3cm wide prostate. Without planning, deformations are ignored and the needle is inserted to $(\bar{y}, \bar{z}) = (y_t, z_t)$, the seed would be implanted at (y, z) = (1.41cm, 2.21cm) in the reference mesh based on our simulation. This results in a placement error E=0.79cm, which is 26% the width of the prostate.

D. Optimizing Insertion Depth

For prostate brachytherapy, we assume that seeds can only be implanted inside the prostate and set $\bar{z}_{max}$ accordingly. We assume needle velocity v is 0.5cm/sec, which is an approximate insertion speed during brachytherapy. The time step is fixed at h=1/30 sec.

Based on standard practice, we first simulate the

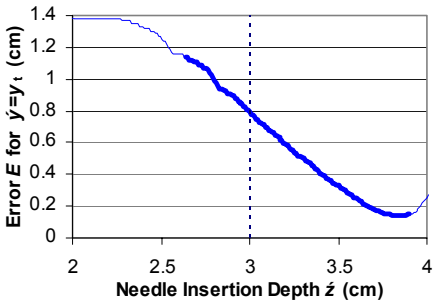

Fig. 5: Needles should generally be inserted deeper than standard practice to compensate for tissue deformations and minimize placement error. Placement error E is plotted as a function of needle insertion depth $\bar{z}$, where the insertion height is fixed at the standard $\bar{y}=y_t$=1.5cm. The bold portion of the line denotes feasible placements inside the prostate. The standard insertion depth $\bar{z}=z_t$=3.0cm yields a placement error of E=0.79cm (26% of prostate width). To minimize error for $\bar{y}=y_t$, the needle should be inserted deeper to a depth of $\bar{z}$*=3.84cm, which yields an error of only E=0.14cm (5% of prostate width).

insertion of a needle at the target height $\bar{y}=y_t$=1.5cm and plot the placement error E as a function of insertion depth in Fig. 5. The standard insertion depth $\bar{z}=z_t$=3.0cm yields a placement error of E=0.79cm, 26% of prostate width. The error in the depth coordinate is caused primarily because the tissue in front of the needle tip is being compressed before it is cut. This means the needle must be inserted deeper than the target depth to decrease this error. To minimize E for $\bar{y}=y_t$, the needle should be inserted deeper to a depth of $\bar{z}$*=3.84cm, which reduces the error by 82% to only E=0.14cm, 5% of prostate width.

E. Optimizing Insertion Height

The prostate is composed of a stiffer material than the surrounding fatty tissue. Because our target is located near the bottom of the prostate, inserting the needle near the target height causes the prostate to rotate slightly clockwise, as shown in Fig. 7. The needle must be inserted higher to compensate for its deflected path through the prostate. Hence, both needle insertion depth and height must be adjusted to eliminate placement error.

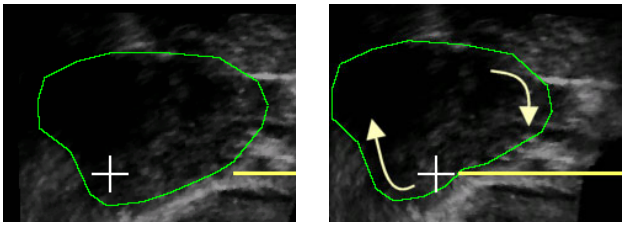

(a) Needle approaches prostate (b) Prostate rotated by needle

Fig. 7: When the needle pushes against the lower half of the prostate from the right, the prostate rotates clockwise slightly because it is stiffer than the surrounding fatty tissue. This slight rotation can lead to significant changes in the optimal needle insertion height.

For a 0.6cm range around the target height $\bar{y}_t$=1.5cm, we plot the computed optimal insertion depth in Fig. 8(a). Fig. 8(b) shows the resulting minimum error E as a

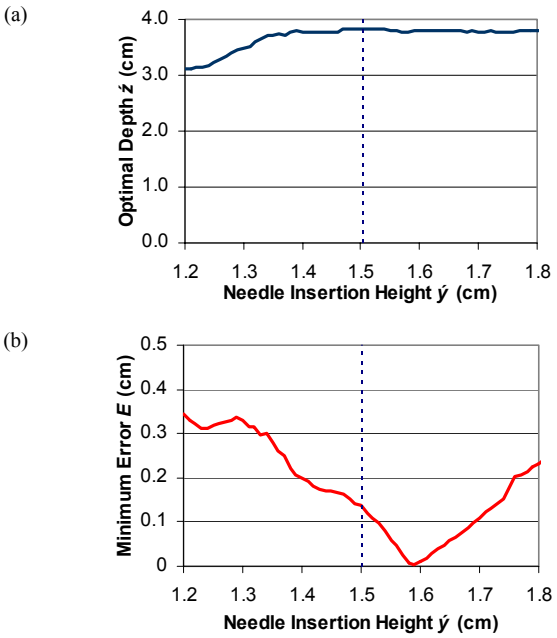

Fig. 8: To eliminate placement error, both needle insertion depth and height must be adjusted. Plot (a) shows the optimal insertion depth $\bar{z}$* computed for different insertion heights. Plot (b) shows the resulting minimum error E as a function of insertion height, assuming that the corresponding optimal depth shown in plot (a) was used. The seed can be placed exactly at the target be inserting at height $\bar{y}$*=1.59cm to a depth of $\bar{z}$*=3.80cm.

function of insertion height, assuming that the corresponding optimal depth shown in plot (a) was used. To compenstate for tissue deformation effects, the needle should be inserted both higher and deeper than standard practice. According to the simulation results, the seed will be placed exactly at the target with E*=0 by inserting at height $\bar{y}$*=1.59cm to a depth of $\bar{z}$*=3.80cm.

The above optimal plan was computed using grid search. As described in section VI.C, we can use the golden section method to find a locally optimal $\bar{y}$* using fewer simulation iterations. To test planner performance, we selected 12 sample points inside the prostate, shown by the crosses in the Fig. 6. We apply the line search in the range $\bar{y}\in(\bar{y}_t$–0.2cm, $\bar{y}_t$+0.2cm) with tolerance 0.01cm

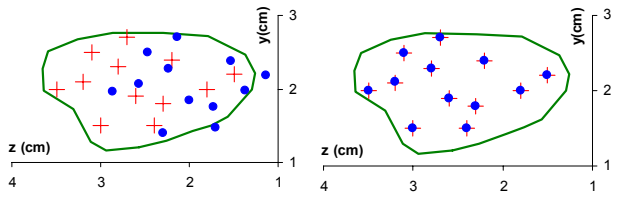

(a) Placements without planning (b) Placements using planner

Fig. 6: Twelve sample points were selected as targets maked "+" inside the prostate. Actual seed placements are marked "•". Standard practice resulted in major placement errors averaging 20% of the prostate width, which will lead to a poor dose distribution (a). Seed placement error was neglible using the planner results (b).

for each target. Using the standard practice approach, the average error was 0.59cm (20% of prostate width) with a standard deviation of 0.10cm. Using our planner, the average error was reduced to 0.002cm (0.1% of prostate width) with a standard deviation of 0.004cm. The average time to compute optimal depth given height was 8.5 seconds and computing both optimal height and depth for a target took an average of 97.7 seconds.

VIII. CONCLUSIONS

In this paper we described a sensorless planning system for needle insertion procedures that incorporates numerical optimization and a soft tissue simulation. The simulation, based on a dynamic FEM formulation, models the effects of needle tip and frictional forces on soft tissues defined by a 2D mesh. Our sensorless planning algorithm for radioactive seed implantation computes needle offsets to minimize seed placement error. The resulting needle offsets compensate for predicted tissue deformations without real-time imaging.

Our planning procedure assumes values for patient-specific parameters such as the Young's modulus. Ideally, seed placement error should be sensitive to physician-controlled parameters and relatively insensitive to patient-specific parameters, since the latter are difficult to estimate before the procedure. The sensitivity analysis in [2] suggests that this is the case: inserting the needle deeper and/or using sharper needles with less surface friction can decrease seed placement error while the variances of the biological parameters of global tissue stiffness and compressibility have only a minimal effect on seed placement error. The effects on placement error of tissue nonhomogeneity and connectivity are currently being examined. Although simulation suggests that planner performance will be relatively insensitive to patient-specific parameters such as global tissue stiffness and compressibility, we will test performance under a variety of conditions using synthetic materials that approximate human tissue before testing on animal and human subjects.

IX. ACKNOWLEDGEMENTS

We thank Russ Taylor for bringing this problem to our attention and Tim Salcudean, Simon DiMaio, Allison Okamura, Dan Halperin, A. Frank van der Stappen, K. Gopalakrishnan, Dezhen Song, Han-Wen Nienhuys, Katja Langen, and Etienne Lessard for their valuable feedback.

X. REFERENCES

[1] R. Alterovitz, J. Pouliot, R. Taschereau, I.C. Hsu, and K. Goldberg, "Simulating needle insertion and radioactive seed implantation for prostate brachytherapy," *Medicine Meets Virtual Reality 11*, J.D. Westwood et al. (Eds.), IOS Press, January 2003, pp. 19-25.

[2] R. Alterovitz, J. Pouliot, R. Taschereau, I.C. Hsu, and K. Goldberg, "Needle insertion and radioactive seed implantation in human tissues: simulation and sensitivity analysis," in *Proc. of the IEEE Int. Conf. on Robotics and Automation*, May 2003. (*Accepted*)

[3] R. Alterovitz and K. Goldberg, "Comparing algorithms for soft tissue deformation: accuracy metrics and benchmarks," June 2002. Available: *http://alpha.ieor.berkeley.edu/ron/research/*

[4] F. S. Azar, D. N. Metaxas, M. D. Schnall, "A deformable finite element model of the breast for predicting mechanical deformations under external perturbations," *Academic Radiology*, Vol. 8, No. 10, 2001.

[5] D.J. Balkcom, E.J. Gottlieb, J. C. Trinkle, "A sensorless insertion strategy for rigid planar parts," in *Proc. IEEE Int. Conf. on Robotics and Automation*, May 2002, pp. 882-7.

[6] M.S. Bazaraa, H.D. Sherali, and C.M. Shetty. Nonlinear Programming: Theory and Algorithms, Second Edition. John Wiley & Sons, Inc. 1993.

[7] K.-F. Böhringer, V. Bhatt, B. R. Donald, and K. Goldberg, "Algorithms for sensorless manipulation using a vibrating surface," *Algorithmica*, 2000, 26: 389-429.

[8] J. Brown, J. Rosen, Y. S. Kim, L. Chang, M. N. Sinanan, B. Hannaford, "In-vivo and in-situ compressive properties of porcine abdominal soft tissues," *Medicine Meets Virtual Reality 11*, J.D. Westwood et al. (Eds.), IOS Press, January 2003, pp. 16-32.

[9] S. Cotin, H. Delingette, and N. Ayache, "Real-time elastic deformations of soft tissues for surgery simulation," *IEEE Trans. on Visualization and Computer Graphics*, Vol. 5, No. 1, 1999.

[10] M. G. Coutinho, P. M. Will, "Using dynamic vector force fields to manipulate parts on an intelligent motion surface," in *IEEE Int. Symposium on Assembly and Task Planning*, 1997, pp.200-5.

[11] J. E. Dawson, T. Wu, T. Roy, J. Y. Gy, and H. Kim, "Dose effects of seeds placement deviations from pre-planned positions in ultrasound guided prostate implants," *Radiol. Oncol.* 32, 1994, pp. 268–270.

[12] S. P. DiMaio and S. E. Salcudean, "Needle insertion modeling and simulation," in *Proc. of the IEEE Int. Conf. on Robotics and Automation*, May 2002, pp. 2098-2105.

[13] M. Erdmann and M. Mason, "An Exploration of Sensorless Manipulation," *IEEE Journal of Robotics and Automation*, Vol. 4, No. 4, August, 1986, pp. 369 - 379.

[14] S. F. Gibson and B. Mirtich. "A survey of deformable modeling in computer graphics," *MERL, TR-97-19*, 1997.

[15] K. Y. Goldberg, "Orienting polygonal parts without sensing," *Algorithmica*, 1993, 10: 201-255.

[16] D. Kalanovic, M. P. Ottensmeyer, J. Gross, G. Buess, S. L. Dawson, "Independent testing of soft tissue visco-elasticity using indentation and rotary shear deformations," *Medicine Meets Virtual Reality 11*, J.D. Westwood et al. (Eds.), IOS Press, January 2003, pp. 137-143.

[17] S.K. Kyriacou, D. Shen, C. Davatzikos, "A framework for predictive modeling of intra-operative deformations: a simulation-based study," *Medical Image Computing and Computer-Assisted Intervention*, Oct. 2000, pp. 634-42.

[18] T. A. Krouskop, T. M. Wheeler, F. Kallel, B. S. Garria, and T. Hall, "Elastic moduli of breast and prostate tissues under compression," *Ultrasonic Imaging*, Vol. 20, 1998.

[19] E. Lee, R. J. Gallagher, and M. Zaider, "Planning implants of radionuclides for the treatment of prostate cancer: an application of mixed integer programming," *Optima*, No. 61, March 1999.

[20] M. Moll, K. Goldberg, M. Erdmann, R. Fearing, "Orienting micro-scale parts with squeeze and roll primitives," *IEEE Int. Conf. on Robotics and Automation*, May 2002.

[21] G. Picinbono, H. Delingette, N. Ayache, "Nonlinear and anisotropic elastic soft tissue models for medical simulation," in *Proc. of the IEEE Int. Conf. on Robotics and Automation*, May 2001, pp. 1370-1375.

[22] J. Pouliot, R. Taschereau, C. Coté, J. Roy, and D. Tremblay, "Dosimetric aspects of permanents radioactive implants for the treatment of prostate cancer," *Physics in Canada* 55(2), 1999, pp. 61-68.

[23] J. Pouliot, D. Tremblay, J. Roy, and S. Filice, "Optimization of permanent 125I prostate implants using fast simulated annealing," *Int. J. Radiat. Onco. Biol. Phys.* 36(3), 1996, pp. 711-720.

[24] M. Shi, Hong L., and G. Tao, "A stereo-fluoroscopic image-guided robotic biopsy scheme," *IEEE Transactions on Control Systems Technology*, Vol. 10, No. 3, May 2002, pp. 309-317.
[25] H. Kataoka, T. Washio, K. Chinzei, K. Mizuhara, C. Simone, and A. M. Okamura, "Measurement of the tip and friction force acting on a needle during penetration," *Medical Image Computing and Computer Assisted Intervention*, Sept. 2002.
[26] R. Taschereau, J. Pouliot, J. Roy, D. Tremblay, "Seed misplacement and stabilizing needles in transperineal permanent prostate implants," *Radiotherapy and Oncology* 55, 2000, pp. 59-63.
[27] R. Taschereau, J. Roy, and J. Pouliot, "Monte Carlo simulations of prostate implants to improve dosimetry and compare planning methods," *Med. Phys.* 26 (9), Sept. 1999.
[28] D. Terzopolous, J. Platt, A. Barr, K. Fleischer, "Elastically deformable models," *Computer Graphics*, Vol. 21, No. 4, 1987.
[29] X. Wu, M.S. Downes, T. Goktekin, and F. Tendick, "Adaptive nonlinear finite elements for deformable body simulation using dynamic progressive meshes," *Eurographics 2001, Computer Graphics Forum*, Vol. 20, No. 3, Sept. 2001, pp. 349-358.
[30] M. Zaider et al., "Treatment planning for prostate implants using magnetic-resonance spectroscopy imaging," *Int. J. Radiation Oncology Biol. Phys.*, Vol. 47, No. 4, 2000.
[31] Y. Zhuang, "Real-time simulation of physically realistic global deformations," Ph.D. thesis, UC Berkeley, 2000.
[32] O.C. Zienkiewicz and R.L. Taylor, *The Finite Element Method*, Fifth Edition, Butterworth-Heinemann, 2000.